Towards registration of optical and MR signal changes in subcutaneous tumor volume *in vivo* after optical skin clearing

Alexei A. Bogdanov Jr.[1,2] Valery V. Tuchin [2,3,4,5], Irina G. Meerovich [2], Natalia I. Kazachkina [2], Victoria V. Zherdeva [2], Ilya D. Solovyev [2], Daria K. Tuchina [2,3,4], Alexander P. Savitsky [2].

[1] University of Massachusetts Medical School, Radiology, Worcester, Massachusetts, United States of America
[2] A.N.Bach Institute of Biochemistry, Federal Research Centre "Fundamentals of Biotechnology", Russian Academy of Sciences, Moscow, Russian Federation
[3] Saratov State University, Saratov, Russian Federation
[4] Tomsk State University, Tomsk, Russian Federation
[5] Institute of Precision Mechanics and Control of the Russian Academy of Sciences, Saratov, Russian Federation

ABSTRACT

The goal of this research was in testing magnetic resonance imaging (MRI) pulse sequences for monitoring local changes of proton relaxation times after the local application of skin optical clearing (OC) compositions in vivo. We used xenograft mouse models of cancer, i.e. nu/nu mice bearing subcutaneous tumors expressing endogenous TagRFP red fluorescent protein marker and tested the changes in fluorescence intensity and lifetime (FL) of the subcutaneous tumor foci after OC application (70% glycerol, 5% DMSO, 25% water) onto the skin. By using time-correlated single photon counting within 20-30 min after the OC we observed: 1) 30-40% increase in the overall photon numbers output; 2) 50 ps increase in the median FL of TagRFP. We subsequently performed tracking of MR signal intensity changes within selected regions of interest (ROI) located close to the skin surface before, during and after OC. The analysis of 1T MR T2-weighted (T2w) fast spin-echo images showed significant quantitative differences between Gaussian noise-normalized MRI signal intensities (Mann-Whitney test, $p<0.05$). Our results suggest that the application of OC may cause: 1) a transient change of the peripheral tumoral microenvironment and as a consequence, FL increase and shortening of mean proton relaxation times within the voxels of subcutaneous tumor (i.e. T2w hypointensity increase); 2) potential microviscosity change due to the permeability for the OC components resulting in shortening of tissue water proton relaxation times. Both processes may be due to glycerol induced water displacement in the tissue and in-depth penetration of DMSO molecules. The results suggest that T2w 1T MRI was useful for semi-quantitative monitoring of MR signal intensity longitudinal changes in the subcutaneous space during and after OC thereby enabling registration of optical and MR signal fluctuations in the same voxels of live tissue.

1. INTRODUCTION

1.1 The significance of tissue optical clearing in imaging applications.

Optical clearing is currently considered as an efficient strategy for increasing the depth of light penetration into the non-transparent media such as biological tissues in experimental optical imaging, which has a great potential in expanding clinical use of optical imaging modalities in diagnostics and therapy [1, 2]. In preclinical research OC has been proven to facilitate quality data generation in multiple optical imaging applications, e.g. diffusion tomography, multiphoton imaging and Raman spectroscopy [3] as well as for applications in therapy [4]. For example, OC enables *in vivo* photoacoustic [5-7]and fluorescent [8, 9] transdermal flow cytometry that potentially enables the detection of rare tumor cells in circulation. Transdermal imaging using optical sectioning through the intact skin of the animals *in vivo* (a combination of confocal and multiphoton microscopy) allows to perform optical imaging of various blood vessel structures in tumors and differentiate between cancer and stromal cells [10-12]. Confocal/multiphoton transdermal microscopy was enabled in the latter case by using the application a gel with a refractive index of 1.34 onto a skin surface [10] that ensured not only the contact between the skin and glass of the lens, but also resulted in OC effect by decreasing

Dynamics and Fluctuations in Biomedical Photonics XVII, edited by Valery V. Tuchin
Martin J. Leahy, Ruikang K. Wang, Proc. of SPIE Vol. 11239, 112390N

the scattering of light. It is known that the fibrous structures in tissues such as skin and muscle cause strong light scattering. This effect is a consequence of the refractive index discontinuities located between the fibers and interstitial fluid. OC is generally aimed at decreasing these discontinuities resulting in better refractive index matching. Refractive index matching effectively reduces the scattering and improving depth penetration of light in the tissue. Overall, the OC effect in non-transparent tissue is a consequence of multiple effects occurring at the level of interaction between water-miscible solvents and macromolecules, their aggregates, various supramolecular structures such as self-assembling tissue fibers of extracellular matrix (collagen, elastin, etc.) as well as the cells that are found in the tissue, blood, extracellular fluid/lymph and carry multiple light-absorbing and scattering centers within cell organelles. In the past it has been demonstrated in near-infrared (NIR) optical coherence tomography experiments that the OC of blood is a result of not only the refractive-index matching but also is a consequence of changes in the size of red blood cells, which affects light attenuation, and in their aggregation in the presence of glycerol (i.e. an experimental OC component), resulting in the light penetration depth increase (in the range of 20-150.5%) [13]. The most detailed description of a hypothetical molecular mechanism of tissue OC within the post-diffusion stage has been a result of computer simulations, i.e. molecular dynamics [14]. However, molecular modeling of the entire spectrum of effects caused by OC in the tissue is not feasible. Therefore, to improve OC protocols in terms of their overall efficacy and biocompatibility it is imperative to: 1) select the OC compositions with low toxicity and high biocompatibility; 2) analyze the effects of OC on various tissue components individually in realistic model systems; 3) investigate the OC effects in living systems (e.g. experimental animal models of human disease). It should be noted that by design the OC effects are expected to be transient while enabling a sufficiently wide spectral and longitudinal (time) window for appropriate number of data points acquisition during the imaging study. Therefore, to perform non-invasive assessment of the interaction between OC composition in a living system the imaging modality of choice should have a sufficient spatiotemporal resolution while having the ability to capture changes of tissue environment in a suitable volume of tissue.

1.2 MRI in detection of tissue solvent interactions.

Magnetic resonance imaging (MRI) is a tomographic technique that utilizes radio wave frequency range, non-ionizing radiation with unlimited depth of penetration in the body. Proton MR is exquisitely sensitive to bulk effects caused by diamagnetic water-miscible solvent administration on proton density and proton spin relaxation changes, and in the case of living tissue these are mostly the protons of water. Moreover, the change of microviscosity of the tissue affected by OC components is affecting free and macromolecule-bound (structured) water in the skin layers and subdermal tissue and fluid compartments. For example, rotational diffusion correlation times of proteins strongly depends the viscosity of the water-DMSO mixture as a function of the amount of DMSO and can vary by a factor of 2 in the relevant concentration range [15]. Due to the sensitivity of MRI to changes of tissue rheology MR elastography became an established approach for measuring the extent of fibrosis and inflammation in the liver [16]. Therefore, the application of OC should be expected to change the relaxation rates of polarized water proton spins. It should be noted that OC is affecting the tissue located only several millimeters away from the skin surface and MR correlative studies are not expected to produce meaningful data at the greater depths. The other limitation is potential presence of MR image artifacts at the tissue boundaries. However, unlike many other non-tomographic imaging techniques MRI provides a global assessment of the tissue of interest. MR imaging generates cross-sectional anatomical maps with sufficient detail that are highly useful for registering the images obtained on the periphery of the body (and potentially the underlying organs) while deeper layers of tissue carry multiple anatomic signatures useful for registering image acquired over time, before and after the administration of OC compositions. In our study we hypothesized that at low external magnetic field strengths (Bo=1-1.5T) the effects arising from the modification of skin and subdermal tissue hydration and viscosity that may cause local increase of paramagnetic species in the tissue are reflected in the change of T2-weighted signal intensity due to water proton relaxation rate shortening, which was not expected to be strongly weighted by T2*-effects. The latter are primarily generated by the presence of paramagnetic components of blood (e.g. deoxyhemoglobin) [17]. Therefore, we set forth to investigate whether there is a quantifiable correlation between the effects resulting from optical clearing (OC) with the changes in T2-weighted (T2w) magnetic resonance (MR) signal measured over the matched skin/tissue area acquired using live mouse models of cancer, i.e. tumor xenografts developed in mice.

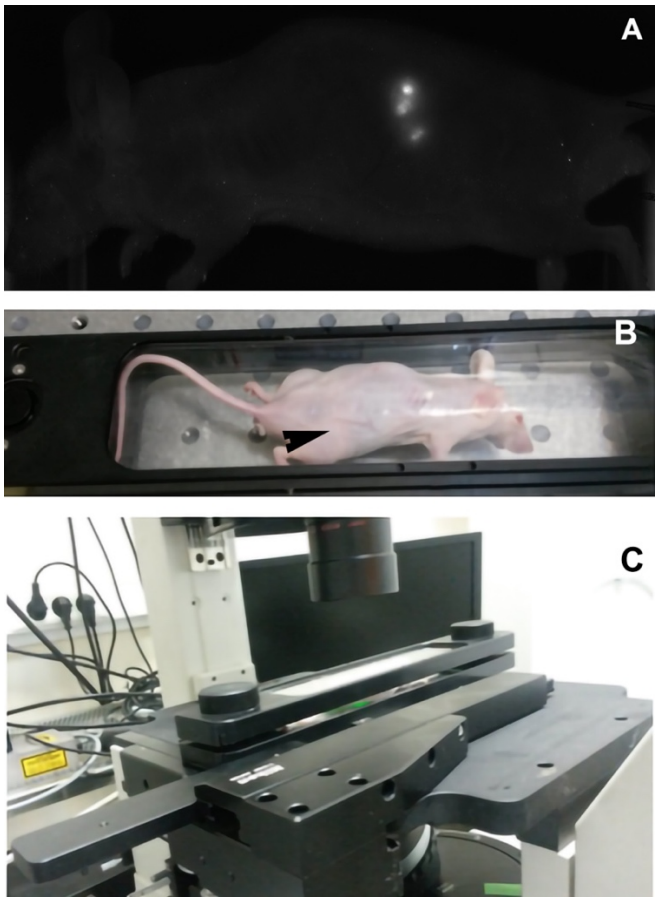

Figure 1. In vivo fluorescence imaging: A – macroscopic low resolution iBox (UVP) image of the whole mouse bearing a HEp-2-TagRFP tumor. The tumor formed three distinct nodules in the mouse flank; B= a cassette for mouse imaging with the tumor in a close proximity to the glass window (indicated by an arrow); C – the cassette positioning on the stage of the confocal in vivo imaging device based on inverted microscope.

2. RESULTS AND DISCUSSION

2.1. Optical Imaging.

The effect of a diamagnetic mixture of glycerol/DMSO/water (the OC mixture) on subcutaneous tissue signal intensity after a short-term application was studied using a non-cryogenic 1T MR imaging system. The OC consisted of a mixture of 70% glycerol, 5% DMSO, 25% water. The OC/MRI experiments were performed in athymic mice (n=5) carrying subcutaneous epithelioid human carcinoma (HEp2 or A549) tumor xenografts expressing Tag RFP, a far-red cell marker protein previously used for sensor engineering and in tumor detection [18, 19]. TagRFP has an emission maximum of 584 nm [20] and it can be imaged *in vivo* at 2-3 weeks after tumor inoculation into the flank of the animals [21]. As previously shown by us the characteristic fluorescence lifetime for TagRFP expressed in HEp2 cells is approximately 2.18 ns [21]. To investigate the effect of OC on image characteristics that reflect the patterns of TagRFP fluorescent protein expression *in vivo* we measured fluorescence intensity (FI) and lifetime (FL) of TagRFP in subcutaneous tumors. Since these tumors appeared very close to the skin surface, we hypothesized that OC should result in the overall increase of FI. The effect of OC on FL is largely unknown. The initial assumption was that because of the decrease of light scattering above the thin subdermal tissue layers as a result of applying the refractive index matching solution FL should result in a decrease of the median FL. Initially we assessed the distribution of subdermal signal on the fluorescence intensity images at low resolution using an iBox camera (Fig. 1A), which in the case of HEp2-TagRFP tumors showed several disseminated subcutaneous tumor nodules. After identifying the precise location of the tumor sources within the peripheral mouse tissue we transferred the mouse under anesthesia into a cassette for macroscopic confocal

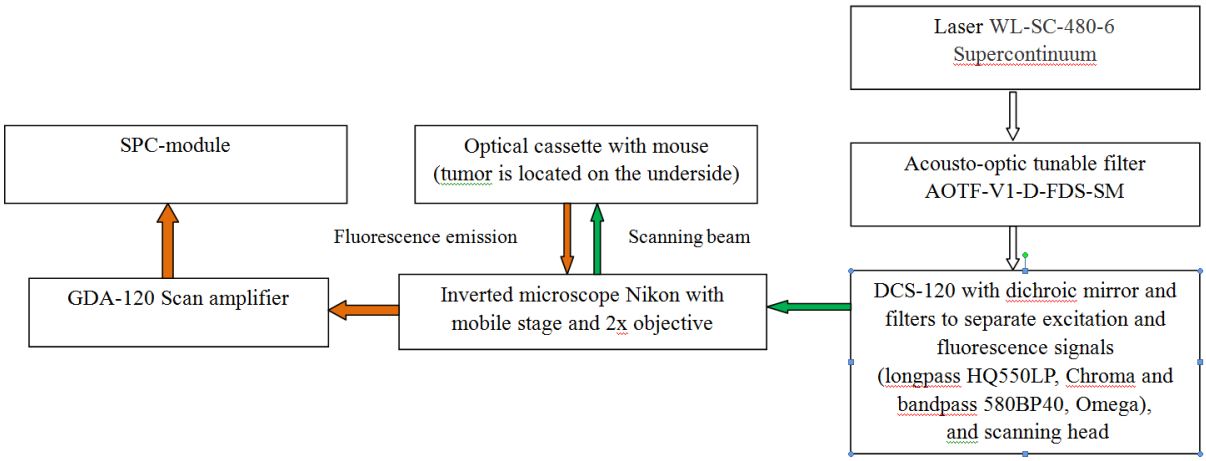

Figure 2. A schematic showing custom macroscopic confocal fluorescence imaging setup.

fluorescence observation and measurements (FI and FL), with tumor nodules immediately adjacent and contacting the glass lid as shown in Figure 1B, arrow. For fluorescence measurements we assembled and used a macroscopic confocal system equipped with a supercontinuum laser with the acousto-optic tunable filter and a photon-counting detector before and after OC, which required inverting the cassette to afford proper lens focusing (Figure 1C). TagRFP fluorescence was excited *in vivo* at 540 nm with additional 510-560 BP accessory filter and the emission was collected by using a HQ550LP (Chroma) and 580BP40 (Omega) filters to cut off the excitation light (Figure 2). Fluorescent signal was recorded through the skin by epi-illumination. The OC effect was achieved by applying the OC mixture onto the skin over the tumor area for 15 min followed by removal of the mixture from the skin and recording confocal images. OC resulted in appreciable increase of tumor brightness as shown on Figure 3A (before) and B (after) representative images of the field shown in Figure 1 taken after a 15 min exposure to optical clearing composition and images were normalized per total number of photons/image. It should be noted that as expected, macroscopic epifluorescent excitation resulted in larger areas of fluorescence than macroscopic confocal fluorescence detection (compare Figures 1A and 3A,B).

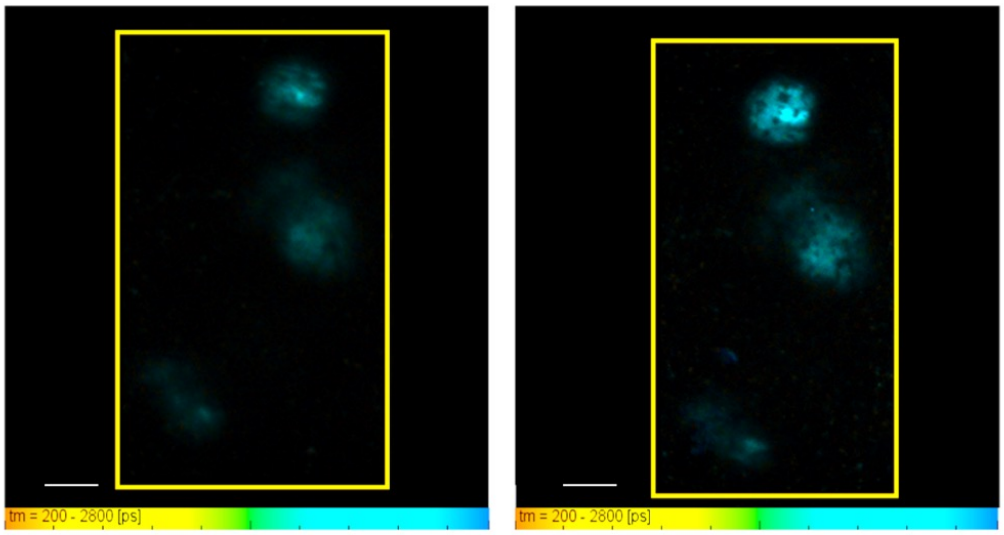

Figure 3. Confocal microscopic image of three small HEp2-TagRFP nodules showing fluorescence intensity of TagRFP before (A) and after (B) of OC application. FL pseudocolor scale is shown under each image. Bar = 1 cm.

However, in multiple cases we observed an overall of more areas of the skin positive for TagRFP fluorescence after OC. To characterize the distribution of emission photons over the spectrum of FL values we collected 20-50·10^3 photons over each ROI and plotted the distribution of registered photons before and after OC, Figure 4A, which shows FL distribution typical for these series of experiments over the entire region of interest (ROI), including both fluorescent tumor foci and the zones around them (that had no specific visible TagRFP fluorescence). Time-correlated single photon counting experiments showed that after OC application FL values characteristic of TagRFP was higher with the median difference of 51 ps ($p<0.05$, Wilcoxon matched-pairs test, Figure 4B). Since the images of tumors clearly appeared more fluorescent after OC, we measured average FI increase, which varied from ROI to ROI. By analyzing determined as increased by 33% after OC) resulting in the higher frequency of fluorescence intensity increase observations (n=19 vs. n=3, Figure 5B).

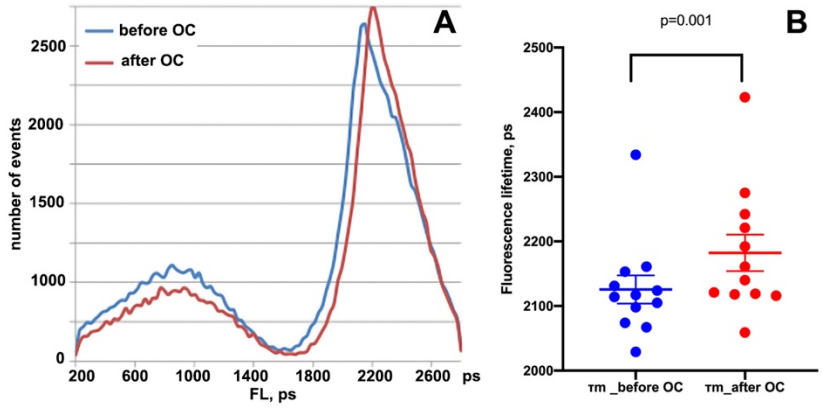

Figure 4. A - Distribution of fluorescence lifetime (FL values) measured across the whole area shown in Figure 3; B – the change of fluorescence lifetime values (in ps) measured using n=3 tumor-bearing animals. TagRFP marker protein FL measured before and after optical clearing (n=12 ROI); FL differences were statistically significant ($p<0.05$) according to Wilcoxon test of paired observation (prior and after optical clearing).

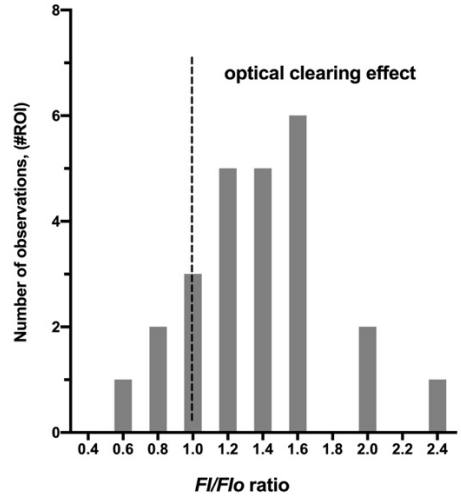

Figure 5. TagRFP fluorescence intensity change histogram showing the observation numbers corresponding to fluorescence intensity ratio changes expressed as F_i/F_o, where F_o is the initial integrated fluorescence intensity of given ROI before OC. Fluorescence intensity increase (i.e. $F_i/F_o>1$) indicating optical clearing effect was detected in 19 ROI out of 22 total in n=3 animals.

2.2 MRI of optical clearing composition effects on imaging signal in the skin and subcutaneous tissue layer.

It is known that OC compositions penetrate through the skin and depending on how efficient this process is the presence of glycerol in those compositions is capable of causing a reverse flow of free or loosely bound water from the skin and gradually replace it over time. The effects of OC components are likely to be dissimilar, depending on the nature of the mixture. In our case the glycerol is likely to affect the tissue differently than DMSO since according to Raman spectroscopy results obtained in a model system [22, 23] glycerol alone does not penetrate into the skin to the depths greater than tens of microns per hour. It is likely that glycerol can affect the water in a remote way by setting water in motion in deeper layers of tissue, i.e. up to 1-2 mm deep. Glycerol thereby may assist in increasing the refractive index of the tissue environment and increase the viscosity of the interstitial fluid due to the withdrawal of water and simultaneous increase the concentration of proteins (including paramagnetic deoxyhemoglobin) and salts dissolved in it. The latter may have direct consequences for MRI signal because it depends on concentration of paramagnetic species as well as tissue microviscosity. We set forth to use the same experimental setup and OC protocol that was described before, i.e. we used the same xenograft-bearing animal treated with OC composition followed by subjecting to MRI before and after the OC application, with MR images acquired over time by using T2w fast spin-echo (FSE) MRI pulse sequences in the same animals shortly after optical imaging. The analysis of obtained T2w FSE MR images showed significant quantitative differences ($p=0.03$) between the Gaussian noise-normalized MR signal intensities of the 0.7-mm-thick axial peripheral tissue/skin slices before and after OC mixture applications in 5 animals (i.e. signal-to-noise ratios, SNR, Table 1). The differences of MR signal were measured by ROI analysis in 6 or more tomographic slices (0.7 mm thick) as shown in Figure 6A. The increase of apparent R2 (transverse relaxation rates) due to the penetration of OC composition through the skin, which results in the measurable "darkening" of the subcutaneous space below the treated skin, i.e. in the tumor periphery. These MR signal changes differences, which are negative in value, indicate the increase of the apparent T2w MR signal (a function of R2). As a result, we observed highly statistically significant changes of T2w MR signal in three out of five animals under study, Table 1 (*P* values, Mann-Whitney test) (Figure 6B). To test, whether the observed T2w signal increase, which is observed as measurable "darkening" of the image could be a potential consequence of OC dilution in the extracellular fluid we conducted phantom experiments. We performed dilutions of OC in water and applied the same T2w FSE pulse sequences to record the change in T2w signal in the obtained samples (Figure 7). We observed no statistically significant differences when we compared T2w MR signal intensities measured in 100% OC, mixture phantoms various dilutions of OC, as well as pure water. This control MRI experiment showed that the observed differences in T2w MR signal intensity were not due to the application of OC mixture because T2w signal decreased (increased in value) upon dilution. Therefore, the dilution is unlikely to be the reason behind the T2w signal increase. It appears that the change in MR signal is instead a consequence of OC mixture interaction with the skin and subcutaneous tissue.

Table 1. Mean SNR and the change of magnetic resonance imaging signal intensity (ΔSI) measured by using T2-weighted fast-spin-echo pulse sequences at 1T.

	HEp-2-TagRFP1		HEp-2-TagRFP2		HEp-2-TagRFP3		A549-TagRFP 1		A549-TagRFP 2	
	before	after	before	after	before	after	before	after	before	after
mean SNR [1)]	49.63	42.02	16.05	14.33	20.05	18.48	14.70	13.10	17.81	16.00
SD	4.33	5.73	0.92	1.85	3.51	1.99	1.77	1.70	0.59	1.87
SEM	1.37	1.73	0.33	0.65	1.01	0.60	0.56	0.57	0.24	0.76
ΔSI		**-7.61**		**-1.72**		-1.57		-1.6		**-1.81**
P [2)]		0.04		0.03		0.06		0.2		0.04

1) Mean normalized MR signal intensity change before and after OC application was measured using T2w FSE pulse sequence (TR/TE 4000/39.8) in 6 or more 0.7 mm thick tomographic slices. $SNR_i = SI_i/SD_{noise}$
2) Mann-Whitney test, n=6-12 data points

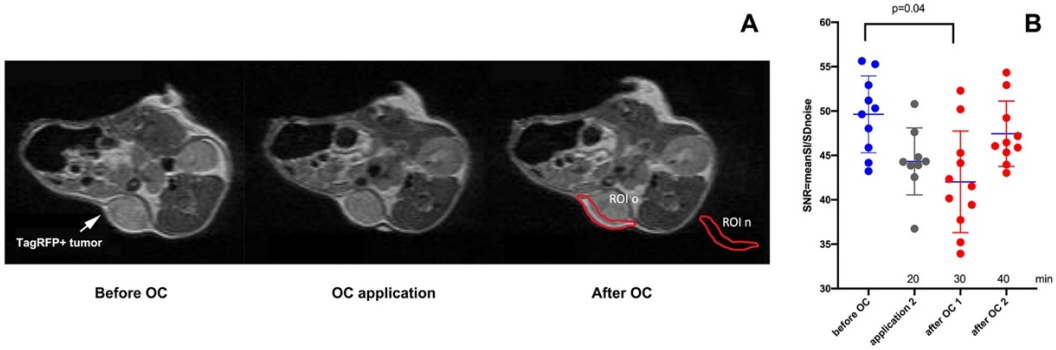

Figure 6: MRI of signal change after OC using T2-weighted fast-spin-echo pulse sequences at 1T. **A**- T2w FSE (TR/TE=4000/40 ms, 7NEX, 0.7 mm slice thickness) of TagRFP expressing tumor-bearing mouse at 1T, before, during and after OC with ROI used to calculate tissue MR signal intensity and SD of noise shown in red; **B**- a representative scatter dot plot showing the change of normalized T2w MR signal intensity in n=10 slices over time before, during and after OC solution application onto the skin of the xenograft-bearing mouse. The mean MR signal intensity±SD is shown along with the measurements in each of the slices.

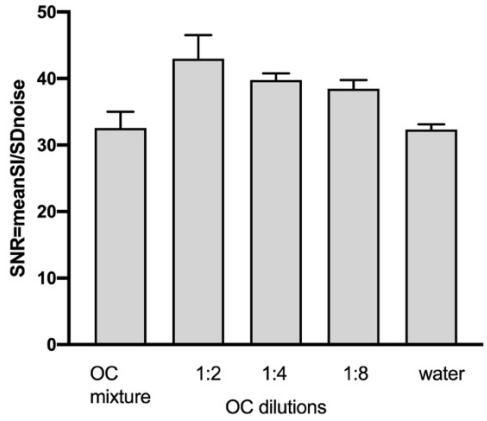

Figure 7: The results of MRI using T2-weighted fast-spin-echo pulse sequences, TR/TE=4000/40 ms, 7NEX, 0.7 mm slice thickness applied to phantoms containing either 100% OC, serially diluted OC, or water.
Normalized signal intensity (SNR) shows identical signal in water and OC and no T2w effect upon dilution.

CONCLUSIONS

The obtained results point to the potential mechanism of OC clearing as it relates to: 1) a transient change of the peripheral tumoral microenvironment affecting the superficial layer of Tag-RFP expressing cells which results in fluorescence intensity increase because of refractive index matching and caused by shortening of mean proton transverse relaxation times within the voxels of subcutaneous tumors; 2) potential increase of blood volume/deoxyhemoglobin concentration due to skin permeability for the OC components and their osmotic properties leading to water displacement and T2w MR hypointensity increase because of the shortening of tissue water proton transverse relaxation times. The phantom experiments suggest that the effect of the OC mixture on MR signal is indirect rather than direct consequence of either OC/water magnetic relaxation properties, or additional chemical shift artifact. Therefore, T2w 1T MRI showed certain promise as a technique suitable for detecting small longitudinal changes of the MR signal in the subcutaneous tissue under the conditions of OC, which resulted in an increase of FI/FL of a red fluorescent marker protein. The latter effects are expected to benefit in vivo imaging of marker protein expression in animal tumor models.

Acknowledgment. The authors are grateful for the financial support for project No. 14.W03.31.0023 to the Ministry of Science and Higher Education of the Russian Federation. This work was supported in part by NIH grants R01DK095728 and R01EB000858 (to A.B.).

References.

1. Genina EA, Bashkatov AN, Tuchin VV. Tissue optical immersion clearing. Expert Rev Med Devices. 2010; 7: 825-42.
2. Sdobnov AY, Darvin ME, Genina EA, Bashkatov AN, Lademann J, Tuchin VV. Recent progress in tissue optical clearing for spectroscopic application. Spectrochim Acta A Mol Biomol Spectrosc. 2018; 197: 216-29.
3. Tuchin VV. Tissue optics: Light scattering methods and instruments for medical diagnosis. Bellingham, WA: SPIE Press; 2015.
4. Alexandrovskaya YM, Evtushenko EG, Obrezkova MM, Tuchin VV, Sobol EN. Control of optical transparency and infrared laser heating of costal cartilage via injection of iohexol. J Biophotonics. 2018; 11: e201800195.
5. Zharov VP, Galanzha EI, Shashkov EV, Khlebtsov NG, Tuchin VV. In vivo photoacoustic flow cytometry for monitoring of circulating single cancer cells and contrast agents. Opt Lett. 2006; 31: 3623-5.
6. Menyaev YA, Nedosekin DA, Sarimollaoglu M, Juratli MA, Galanzha EI, Tuchin VV, et al. Optical clearing in photoacoustic flow cytometry. Biomed Opt Express. 2013; 4: 3030-41.
7. Galanzha EI, Kokoska MS, Shashkov EV, Kim JW, Tuchin VV, Zharov VP. In vivo fiber-based multicolor photoacoustic detection and photothermal purging of metastasis in sentinel lymph nodes targeted by nanoparticles. J Biophotonics. 2009; 2: 528-39.
8. Patil R, Tan X, Bartosik P, Detappe A, Runnels JM, Ghobrial I, et al. Fluorescence monitoring of rare circulating tumor cell and cluster dissemination in a multiple myeloma xenograft model in vivo. J Biomed Opt. 2019; 24: 1-11.
9. Pitsillides CM, Runnels JM, Spencer JA, Zhi L, Wu MX, Lin CP. Cell labeling approaches for fluorescence-based in vivo flow cytometry. Cytometry A. 2011; 79: 758-65.
10. Bogdanov AA, Jr., Lin CP, Simonova M, Matuszewski L, Weissleder R. Cellular activation of the self-quenched fluorescent reporter probe in tumor microenvironment. Neoplasia. 2002; 4: 228-36.
11. Runnels JM, Zamiri P, Spencer JA, Veilleux I, Wei X, Bogdanov A, et al. Imaging molecular expression on vascular endothelial cells by in vivo immunofluorescence microscopy. Mol Imaging. 2006; 5: 31-40.
12. Bogdanov AA, Jr., Lin CP, Kang HW. Optical imaging of the adoptive transfer of human endothelial cells in mice using anti-human CD31 monoclonal antibody. Pharm Res. 2007; 24: 1186-92.
13. Tuchin VV, Xu X, Wang RK. Dynamic optical coherence tomography in studies of optical clearing, sedimentation, and aggregation of immersed blood. Appl Opt. 2002; 41: 258-71.
14. Berezin KV, Dvoretski KN, Chernavina ML, Likhter AM, Smirnov VV, Shagautdinova IT, et al. Molecular modeling of immersion optical clearing of biological tissues. J Mol Model. 2018; 24: 45.
15. Wallerstein J, Akke M. Minute Additions of DMSO Affect Protein Dynamics Measurements by NMR Relaxation Experiments through Significant Changes in Solvent Viscosity. Chemphyschem. 2019; 20: 326-32.
16. Sinkus R, Lambert S, Abd-Elmoniem KZ, Morse C, Heller T, Guenthner C, et al. Rheological determinants for simultaneous staging of hepatic fibrosis and inflammation in patients with chronic liver disease. NMR Biomed. 2018; 31: e3956.
17. Farahani K, Sinha U, Sinha S, Chiu LC, Lufkin RB. Effect of field strength on susceptibility artifacts in magnetic resonance imaging. Comput Med Imaging Graph. 1990; 14: 409-13.
18. Rusanov AL, Ivashina TV, Vinokurov LM, Fiks, II, Orlova AG, Turchin IV, et al. Lifetime imaging of FRET between red fluorescent proteins. J Biophotonics. 2010; 3: 774-83.
19. Savitsky AP, Rusanov AL, Zherdeva VV, Gorodnicheva TV, Khrenova MG, Nemukhin AV. FLIM-FRET Imaging of Caspase-3 Activity in Live Cells Using Pair of Red Fluorescent Proteins. Theranostics. 2012; 2: 215-26.
20. Merzlyak EM, Goedhart J, Shcherbo D, Bulina ME, Shcheglov AS, Fradkov AF, et al. Bright monomeric red fluorescent protein with an extended fluorescence lifetime. Nat Methods. 2007; 4: 555-7.
21. Zherdeva V, Kazachkina NI, Shcheslavskiy V, Savitsky AP. Long-term fluorescence lifetime imaging of a genetically encoded sensor for caspase-3 activity in mouse tumor xenografts. J Biomed Opt. 2018; 23: 1-11.
22. Darvin ME, Schleusener J, Parenz F, Seidel O, Krafft C, Popp J, et al. Confocal Raman microscopy combined with optical clearing for identification of inks in multicolored tattooed skin in vivo. Analyst. 2018; 143: 4990-9.
23. Sdobnov AY, Darvin ME, Schleusener J, Lademann J, Tuchin VV. Hydrogen bound water profiles in the skin influenced by optical clearing molecular agents-Quantitative analysis using confocal Raman microscopy. J Biophotonics. 2019; 12: e201800283.